Available online at www.sciencedirect.com
SCIENCE DIRECT®
Combustion and Flame 140 (2005) 310–318
Combustion and Flame
www.elsevier.com/locate/combustflame

Effect of polymorphic phase transformations in Al_2O_3 film on oxidation kinetics of aluminum powders

Mikhaylo A. Trunov, Mirko Schoenitz, Xiaoying Zhu, Edward L. Dreizin *

Department of Mechanical Engineering, New Jersey Institute of Technology, Newark, NJ 07102-1972, USA

Received 14 June 2004; received in revised form 18 October 2004; accepted 18 October 2004

Available online 6 January 2005

Abstract

Thermogravimetry was used to study the oxidation of aluminum powders at elevated temperatures. Aluminum powders of various particle sizes and surface morphologies were heated in oxygen up to 1500 °C at different heating rates. Partially oxidized samples were recovered from selected intermediate temperatures and the oxide phases present were analyzed by X-ray diffraction. The experimental data were related to current information on stabilities and phase changes of Al_2O_3 polymorphs. Aluminum powders were observed to oxidize in four distinct stages in the temperature range from 300 to 1500 °C. During stage I, from 300 to about 550 °C, the thickness of the natural amorphous alumina layer on the particle surface increases. The rate of this process is controlled by the outward diffusion of Al cations. At about 550 °C, when the oxide layer thickness exceeds the critical thickness of amorphous alumina of about 4 nm, the oxide transforms into γ-Al_2O_3. The specific volume of γ-Al_2O_3 is less than that of amorphous alumina; therefore, the newly formed γ-Al_2O_3 only partially covers the aluminum surface. The oxidation rate increases rapidly at the onset of stage II, but it decreases when the γ-Al_2O_3 layer becomes continuous. During stage III oxidation, the γ-Al_2O_3 layer grows and partially transforms into the structurally similar θ-Al_2O_3 polymorph. Finally, oxidation stage IV is observed after the transition to stable α-Al_2O_3 results in an abrupt reduction of oxidation rate. Qualitative analysis of the rates of oxidation at the different stages enables one to understand the wide range of aluminum ignition temperatures observed for particles of different sizes.

Keywords: Aluminum ignition; Aluminum oxidation; TGA; Al_2O_3 polymorphs

1. Introduction

Aluminum is widely used as a fuel additive in propellants, explosives, and pyrotechnics. The processes of its combustion have been studied extensively, e.g., [1–3]; however, some of the processes that are crucial for accurate modeling of aluminized energetic materials remain poorly understood. The ignition of aluminum particles is one such process. Aluminum oxide film, always present on the particle surface, is well known for its protective properties. It prevents oxidation of aluminum and its alloys at low temperatures. At elevated temperatures, the properties of the oxide must change, leading up to ignition, but this evolution of the oxide film during particle heating has never been systematically studied. Currently, a commonly accepted idea linking oxide evolution and

* Corresponding author. Fax: +1-973-642-4282.
E-mail address: dreizin@njit.edu (E.L. Dreizin).

0010-2180/$ – see front matter
doi:10.1016/j.combustflame.2004.10.010

ignition is that aluminum particles ignite at or in the vicinity of the Al_2O_3 melting point (2054 °C), when the integrity of the surface coating is destroyed either because of melting or because of the mounting mechanical stresses [4,5]. While a number of investigators have indeed observed aluminum ignition to occur in the vicinity of 2000 °C, e.g., [6–9], the review of the literature shows that aluminum particles could be ignited in a wide range of temperatures. In recent reports on combustion properties of aluminum nanopowders, ignition was observed to occur at temperatures of about 800 °C [10] or lower. Ignition of different micrometer-sized aluminum powders was reported to occur in the temperature range of 650–2000 °C [11–15]. A summary of some of the available reports on aluminum ignition in oxygen-containing environments is presented in Fig. 1, where the observed ignition temperatures are plotted against the size of the tested aluminum samples. The ignition observed at temperatures well below the alumina melting point can only be explained by taking into account the exothermic heterogeneous reactions that occur despite the protective alumina coating. Attempts have been made to consider such reactions using a simplified single-term Arrhenius-type expression [16–18]. Activation energies describing kinetics of such a heterogeneous reaction were adopted from early aluminum oxidation studies. However, the values reported in literature vary widely (from 78 kJ/mol [19] to 418 kJ/mol [20]) and no justification has been provided for the selection of any particular value to model ignition. Moreover, it has been shown clearly that the reaction kinetics of aluminum are complex and cannot be described by simple, single-term rate equations [21].

In this paper, a brief summary of the changes known to occur in aluminum oxide films is presented and the oxidation of aluminum powders with different particle sizes is studied experimentally. The results are analyzed to identify the processes affecting aluminum oxidation rates at different temperatures and also to interpret qualitatively the experimental observations that show ignition of aluminum powders occurring over a wide temperature range.

2. Background: phase changes in growing alumina scales

Aluminum oxide phases and phase changes have been extensively studied and excellent reviews, e.g., [22] are available in literature. Significant progress has also been made recently in understanding the growth kinetics of alumina layers at elevated temperatures [23–25] and in the quantification of related mass transfer coefficients, e.g., review [26]. Because this information has not been used extensively by combustion researchers, a brief summary is given below.

A thin, amorphous layer of alumina forms on the aluminum surface at room temperature [23,24]. The thickness of this “natural” oxide coating (also referred to as “limiting” oxide film thickness) has been evaluated by different researchers as varying from about 0.5 nm [25] to 4 nm [27], while most of the authors suggest a thickness of 2–3 nm, e.g., [28–30]. Growth of the amorphous oxide layer is limited by the outward diffusion of aluminum cations [25]. It has been found that until the thickness of the layer reaches a critical value, the amorphous alumina is thermodynamically more stable on the aluminum surface than crystalline aluminum oxides [23]. The critical thickness depends on the crystallographic orientation of the aluminum substrate and varies somewhat as a function of temperature. In the temperature range 20–600 °C, specific values are close to 0.5, 2.5, and 5 nm for the 111, 100, and 110 crystallographic faces of aluminum, respectively [23]. After the critical thick-

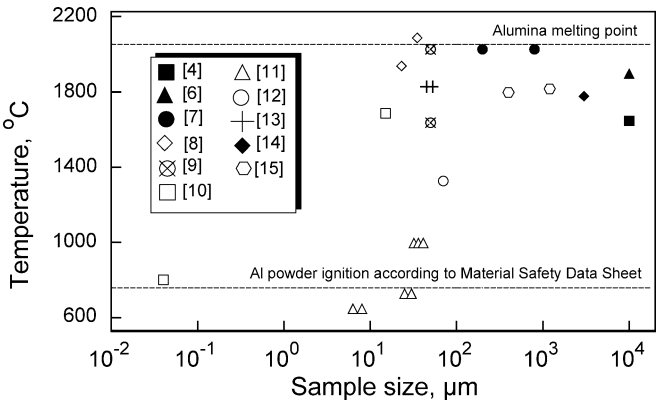

Fig. 1. Summary of the aluminum ignition temperatures reported in the literature.

ness of the amorphous alumina layer is exceeded, it becomes metastable and transitions to γ-alumina. The resulting γ-alumina is stabilized due to its small crystallite size [31]. A network of grain boundaries within the γ-alumina scale provides short-circuit diffusion paths for oxygen [26]. Thus, inward oxygen diffusion becomes the rate-limiting mechanism for the growth of γ-alumina scales [25,26]. When the temperature increases to about 950–1250 °C [22], γ-alumina transforms into thermodynamically stable α-alumina. This transformation may proceed directly or via intermediate phases, such as δ- and θ-alumina [22]. The formation of α-alumina crystallites with larger dimensions (exceeding 30 nm) and higher density results in the overall densification of the alumina scale and in slower oxide growth [22]. The grain boundary diffusion of oxygen toward the Al–Al_2O_3 interface remains the oxidation rate-limiting process.

3. Materials and methods

Four types of aluminum powders were used in this study. Representative electron microscope images of the particles are shown in Fig. 2. Two fine powders have nearly ideal spherical particles: Alfa Aesar, nominal size 3–4.5 μm (97.5% Al), and 10–14 μm (98% Al). A coarser aluminum powder, Alfa Aesar $-40 + 325$ mesh, has particles with irregular shapes. The fourth sample used was aluminum flakes by Iowa Pyro Supply, -325 mesh. The flakes are from 20 to 200 nm thick.

The particle sizes were analyzed using low-angle laser light scattering (LALLS; LS230 Beckman–Coulter Particle Analyzer) for all samples except flakes. Specific surfaces of the finer powders, S_{BET}, were measured by the Brunauer–Emmett–Teller (BET) method using a NOVA 3000 high-speed gas sorption analyzer. The BET diameters, d_{BET}, were calculated as $d_{BET} = 6/(S_{BET}\rho_{Al})$, where ρ_{Al} is the density of aluminum. The measured particle sizes are presented in Table 1.

The oxidation of aluminum powder in oxygen was studied by differential thermal analysis (DTA) with simultaneous thermogravimetric analysis (TGA) using a Netzsch simultaneous thermal analyzer STA409 PC. The instrument was calibrated for temperature with the melting points of a set of metal standards resulting in a temperature accuracy of ±1 °C. Samples of 25–30 mg contained in alumina crucibles were heated from room temperature to 1490 °C with heating rates varying from 5 to 40 °C/min in different experiments. The oxygen flow rate was 50 ml/min. To recover the intermediate products, in some experiments the sample oxidation was interrupted at a particular temperature, the oxygen atmosphere was replaced with argon, and samples were cooled to room temperature. Recovered samples of intermediate products were an-

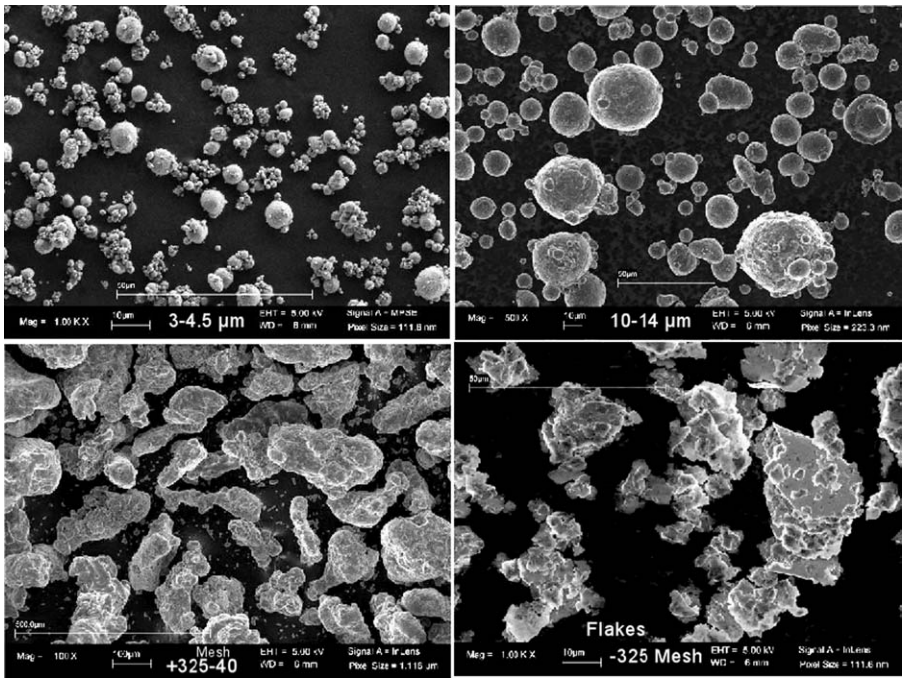

Fig. 2. SEM images of the aluminum powders used in oxidation experiments.

Table 1
Characteristics of used aluminum powders

Powder ID	Specific surface, S_{BET}, m^2/g	BET diameter, d_{BET}, μm	Laser light scattering: Area mean diameter, μm
Spheres 3–4.5 μm	1.15	1.93	3.9
Spheres 10–14 μm	0.41	5.42	16.4
−40 + 325 mesh	N/A	N/A	201.1
Flakes −325 mesh	7.41	N/A	N/A

alyzed by X-ray diffraction (XRD) on a Philips X'pert MRD X-ray diffractometer using unfiltered Cu$K\alpha$ radiation ($\lambda = 1.54187$, 45 kV, 40 mA). The samples were thinly coated on a single-crystal Si sample holder using hexane as a dispersion medium; diffraction patterns were collected from 15° to 70° 2θ.

4. Results

The TGA curves in Fig. 3 show the sample mass increase as a function of temperature for different aluminum powders heated at different heating rates. At temperatures below ∼550 °C, the oxidation is relatively slow; a significant mass increase (of about 5%) was observed only for aluminum flakes, which have the highest specific surface of the powders studied (comparable to that of aluminum nanopowders, e.g., [32]). Accelerated oxidation was consistently observed for all samples in a narrow temperature range from 550 to 650 °C. Oxidation slowed down significantly just before the aluminum melting point. Insets in Fig. 3 show this region of the TGA curves with a magnified vertical scale. For the aluminum flakes heated at 5 K/min, this increased oxidation rate resulted in the oxidation of more than a third of all the available aluminum. The sample of Al flakes heated at 10 K/min ignited during the experiment at about 560 °C as illustrated by a very sharp weight increase.

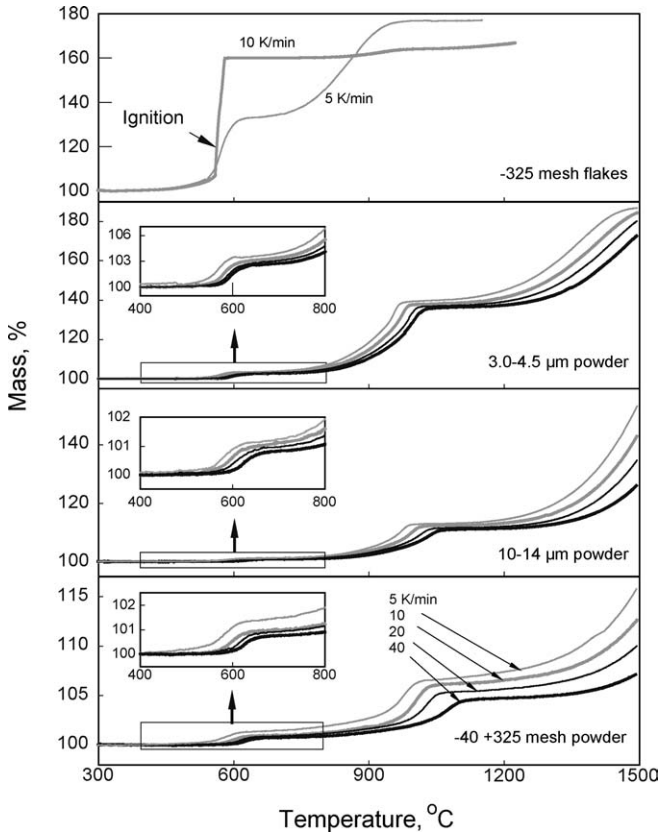

Fig. 3. Summary of TGA measurements for oxidation of different aluminum powders.

This stepwise oxidation was completed for all samples by about 650 °C. At this temperature, the oxidation rate was at its minimum and started to continuously increase while the temperature was increased up to about 1000–1100 °C. Note that the complete oxidation to Al_2O_3 would result in a mass increase of about 88%. In the case of flakes, nearly all the aluminum was oxidized below 1000 °C, and the oxidation rate slowly decreased as the temperature continued to increase. For other powders, a fairly thick oxide layer was formed by about 1100 °C, at which point the oxidation rate decreased abruptly. Very low oxidation rates are inferred for all of the powders by the nearly horizontal portions of the TGA curves between about 1100 and 1200 °C. Continuing temperature increase resulted again in an accelerated oxidation. The measurements above 1450 °C were generally less reproducible and should be regarded with caution because of the approaching limit of the temperature calibration range (1500 °C).

The qualitative oxidation behavior described above was consistently observed for all powders. At higher heating rates, the observed oxidation steps consistently shifted toward higher temperatures as illustrated in Fig. 3. The processing of the experimental data using isoconversion methods was attempted in order to evaluate the activation energies of different oxidation steps, e.g., in the vicinity of 600 and 1050 °C. This processing was not successful: the values of the obtained activation energies were inconsistent from sample to sample in spite of qualitative similarities between the TGA curves for different powders.

Below, different regions of the TGA curves are referred to in terms of oxidation stages. These stages are shown schematically in Fig. 4 using a typical TGA curve and its derivative, which is directly proportional to the rate of oxidation. The first stage refers to the slow oxidation at temperatures below ∼550 °C. The

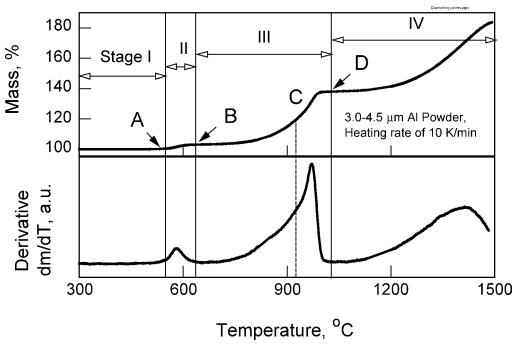

Fig. 4. Stages in oxidation of aluminum powders: a typical TGA curve and its derivative as a function of temperature. Points A, B, C, and D show temperatures at which the samples were recovered for XRD analyses.

second stage describes the stepwise mass increase in the temperature range 550–650 °C. The third stage describes the temperature interval over which the oxidation rate continuously increases, from about 650 to 1000–1100 °C. The increase of the oxidation rate is abruptly terminated, as is clearly shown by the derivative of the TGA curve in Fig. 4. Finally, the fourth oxidation stage describes the increase of the oxidation rate above 1100 °C.

In order to understand the processes causing the observed changes in the oxidation rate and to identify intermediate oxidation products, several samples of spherical aluminum with particle size 3–4.5 μm were heated in oxygen at 10 °C/min to selected temperatures, cooled in argon, and analyzed by XRD. Samples were recovered from 540, 635, 926, and 1020 °C, as illustrated in Fig. 4 by points A, B, C, and D, respectively. Since the mass increase for the spherical powder during the first oxidation stage was very small, a sample of aluminum flakes containing significantly larger amounts of oxide (see Fig. 3) was also heated to 540 °C and recovered for analysis.

The X-ray patterns of samples oxidized to different temperatures are shown in Fig. 5. The patterns are not shown for the samples oxidized to 540 °C because no peaks of Al_2O_3 could be identified for either the spherical powder or the flakes. Weak peaks of γ-Al_2O_3, in addition to strong peaks of metallic aluminum, are observed for the sample recovered from 635 °C. The peaks of α-Al_2O_3 become noticeable only by the end of the third oxidation stage, at 926 °C. At this point, the peaks of γ-Al_2O_3 become stronger and a set of peaks corresponding to θ-Al_2O_3 appear. The peaks of γ-Al_2O_3 disappear from the XRD patterns upon completion of the third oxidation step, at 1020 °C. At this point, the peaks of α-Al_2O_3 become very strong, and only minute amounts of θ-Al_2O_3 remain.

The thickness of the oxide layer at different oxidation stages was estimated from the increase in the overall sample mass as observed in the TGA curves. For this simple estimate, the oxide was assumed to uniformly cover the powder surface area determined by BET. The thickness of oxide film for the flakes was also estimated using the BET specific surface measurements and assuming that the flake thickness is significantly smaller than its length and width. Note that specific surface of the coarse, $-40 + 325$ mesh powder was smaller than could be determined by BET measurements; consequently, the oxide thickness could not be estimated for this powder, either. Based on the phases identified by XRD (see discussion below), the Al_2O_3 layer thicknesses by the end of different oxidation stages were estimated using the density of amorphous alumina for the first oxidation stage ($\rho_{am} = 3050$ kg/m^3 [22]), the density of γ-Al_2O_3

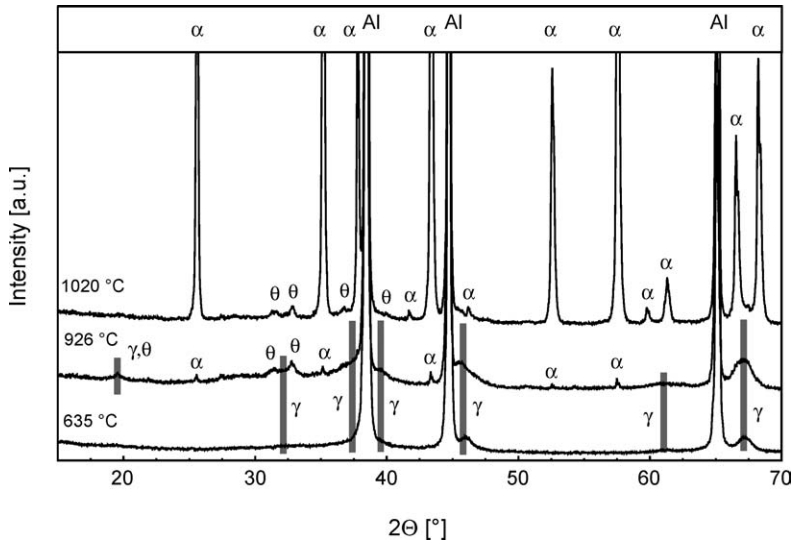

Fig. 5. XRD patterns for partially oxidized aluminum powder samples. The observed XRD peaks are identified for different polymorphs of Al_2O_3.

Table 2
Experimental oxide thickness estimated based on the measured weight increase and powder specific surface from the BET measurements

Powder ID	Heating rate, °C/min	Estimated oxide thickness, nm			
		End of stage I	End of stage II	End of stage III	Stage IV (1450 °C)
Flakes −325 mesh	5	7.4	27.8	N/A, nearly complete oxidation	
	10	8.9		N/A, ignition	
Spheres 3–4.5 μm	5	5.2	20.0	213	707
	10	3.8	18.1	202	567
	20	3.6	16.6	197	480
	40	3.9	15.2	192	395
Spheres 10–14 μm	5	4.7	17.2	176	613
	10	4.2	16.3	168	478
	20	4.6	15.4	155	379
	40	4.0	13.8	149	287

for the second stage ($\rho_\gamma = 3660$ kg/m^3 [22]), and the density of α-Al_2O_3 for the third and fourth oxidation stages ($\rho_\alpha = 3990$ kg/m^3 [22]). The fourth oxidation stage was never completed in these experiments; therefore, the final oxide thickness was estimated at 1450 °C for all powders. The estimated thicknesses of the oxide layers corresponding to the ends of the respective oxidation stages are summarized in Table 2.

5. Discussion

The specific processes responsible for the individual oxidation stages of aluminum powders must be understood in order to accurately model aluminum ignition. The oxidation stages observed in this work are generally consistent with previous reports on aluminum powder oxidation, e.g., [33–35]. Experimental results obtained in this work systematically cover powders with a range of particle sizes and morphologies. This information can be used to develop a qualitative and quantitative description of the oxidation processes involved.

As prepared, aluminum powders are coated with an amorphous alumina layer [22–25]. Therefore, growth of this layer is expected to occur during the initial oxidation stage. The growth of amorphous oxide during stage I oxidation is also consistent with our inability to identify any alumina phases by XRD,

even for partially oxidized sample of aluminum flakes that gained up to 5% of its initial mass during stage I oxidation (see Fig. 3).

The amorphous alumina layer becomes metastable when its thickness exceeds a critical value [23]. A sharp increase in the oxidation rate is indeed observed for both spherical powders when the thickness of the oxide exceeds 3.6–5.2 nm (see Table 2; end of stage I data). This experimentally observed oxide thickness agrees well with the maximum critical thickness of amorphous alumina reported in Ref. [23]. Thus, the transition from stage I to stage II oxidation can be interpreted as the transformation of amorphous alumina to a crystalline alumina polymorph. Note that by end of stage I oxidation, the estimated oxide film thickness for the flake samples is slightly higher than that observed for spherical powders. This minor discrepancy could be caused by the particle surface morphology that was not accounted for in our estimate for the oxidizing surface for flakes.

According to Ref. [22], a common route for the formation of stable α-Al_2O_3 from amorphous alumina film is *amorphous* $\rightarrow \gamma \rightarrow [\delta] \rightarrow [\theta] \rightarrow \alpha$-$Al_2O_3$. The intermediate phases shown in brackets may or may not be produced. The formation of γ-Al_2O_3 is expected during the second oxidation step. The density of γ-Al_2O_3 is about 20% higher than that of amorphous oxide. At the same time, the smallest crystallite size of γ-Al_2O_3 has been observed to be in the range of several nanometers, i.e., comparable to the thickness of the oxide film existing at this point on the aluminum surface. Thus, it is suggested that the newly formed γ-Al_2O_3 scale does not fully cover the aluminum particle surface that was previously protected by continuous amorphous alumina film. The formation of bare aluminum spots, and their immediate oxidation could cause the rapid rate increase of aluminum oxidation at relatively low temperatures in stage II; see Figs. 3, 4. As oxidation continues, the openings in the γ-Al_2O_3 layer heal until a continuous γ-Al_2O_3 coverage forms on the particle surface. This causes the transition to a slower oxidation at the beginning of the observed stage III. According to our measurements, the healing of the γ-Al_2O_3 layer is completed when its equivalent thickness as estimated from the mass increase approaches 15–20 nm. The XRD data confirm the presence of γ-Al_2O_3 by the end of stage II, in agreement with the proposed oxidation mechanism. Note that the detection of broad and relatively small peaks produced by the thin γ-Al_2O_3 layer is difficult. Therefore, only the fine powders with larger relative fractions of oxides were examined in this study using XRD.

Further temperature increase results in continuous growth of the γ-Al_2O_3 layer and its eventual transformation to α-Al_2O_3 via the intermediate transition alumina phases. The presence of θ-Al_2O_3 is clearly established by XRD for the sample recovered from the partially completed stage III (see Figs. 4 and 5). This indicates that stage III may need to be divided further into substages, in which transitions between γ-Al_2O_3 and other metastable alumina polymorphs occur. Note that the densities of the γ, δ, and θ phases are all close to one another [22], so no dramatic changes in the grain boundary oxygen diffusion rate are expected. This diffusion process controls the oxidation rate, which remains almost constant while these polymorphs are being formed. By the end of stage III, the rate of oxidation is dramatically decreased, which can be explained by the formation of a significantly denser and coarser crystallites of α-Al_2O_3. The densification of the alumina layer can readily explain the decrease in the rate of oxygen diffusion and the resulting low rate of alumina growth at the beginning of the stage IV. The XRD pattern once again supports this mechanism showing formation of large quantities of α-Al_2O_3, no γ-Al_2O_3, and only traces of θ-Al_2O_3 at the beginning of stage IV (see Fig. 5). A further temperature increase results in continuously increased rates of oxygen diffusion and oxidation, as observed during the remainder of stage IV.

The oxidation mechanism described above can qualitatively explain why aluminum particle ignition may occur over a wide temperature range. For the simplest analysis of a metal particle ignition in a practical combustion system, one should compare the rate of particle heating by external sources as it enters the flame zone and the rate of particle self-heating due to oxidation. Particle heat losses are neglected in this simplified analysis. When the rate of particle self-heating becomes dominant and the energy released during an oxidation stage becomes sufficient to heat the particle to high temperatures characteristic of aluminum combustion, the ignition criterion is fulfilled. In the experiments discussed in this paper, the external heating rate was completely determined by the settings of the thermal analyzer and was not a function of particle size. Similarly, when micrometer-sized (or finer) particles enter the flame, their heating rate is largely determined by their position in respect to the flame zone and is only slightly affected by particle size. In other words, the particles follow the gas flow fairly closely in terms of both their velocity and temperature. Thus, for a qualitative analysis, the external heating rate could be considered as a constant for particles of different sizes igniting in the same experimental configuration. At the same time, the ratio of the heat release due to oxidation over the particle heat capacity depends on the particle size because smaller particles self-heat more effectively. The diagram in Fig. 6 shows schematically the constant rate

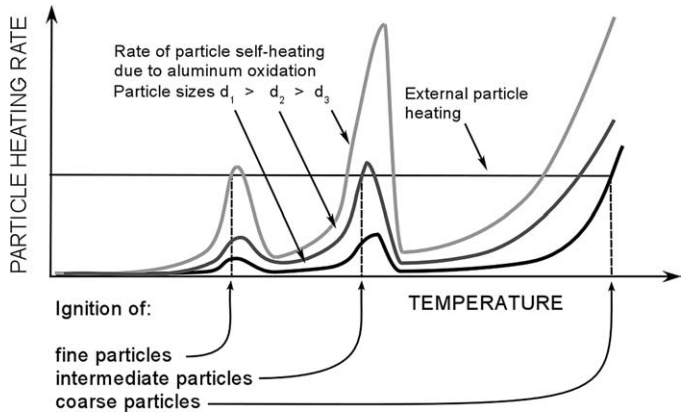

Fig. 6. Schematic diagram comparing the rates of particle self-heating due to particle oxidation against external heating rate for different size metal particles introduced in a combustion chamber. It is suggested that the ignition is observed when the rate of heat release due to particle oxidation starts to dominate in the particle heat balance. The diagram illustrates that ignition of particles of different sizes can be triggered at different oxidation stages and at widely different temperatures.

of external particle heating and three curves showing the rates of particle self-heating as a function of temperature. The self-heating curves imitate the TGA derivative shown in Fig. 4 and are shown schematically for particles of different sizes. Fig. 6 clearly illustrates that the external heating and self-heating curves could cross at different temperatures, depending on the particle size and the external heating rate. For the specific examples shown in Fig. 6, ignition at low temperatures could be observed due to the self-heating peak during stage II oxidation. Ignition at intermediate temperatures could be caused by the peak of stage III oxidation. Ignition at high temperatures could be observed during stage IV when the oxidation rate is increased in the vicinity of the Al_2O_3 melting point. It is suggested that the first case is typical for aluminum nanopowders, the second case describes the ignition of aluminum particles with characteristic dimensions of several micrometers, and the third case is more typical for coarser powders. Clearly, heating rates and other specific features of the experimental system, such as mechanisms of particle heat transfer during the temperature runaway processes, would have a significant effect on the specific ignition temperatures.

In summary, the above discussion suggests that the widely varying ignition temperatures observed for the aluminum powders with distinctly different particle sizes (as shown in Fig. 1) could result from aluminum particle self heating caused by processes associated with different oxidation stages. A more detailed analysis of the experimental data presented in this paper is needed to develop a quantitative aluminum ignition model; this will be the topic of a separate manuscript.

6. Conclusions

Oxidation of aluminum powders at elevated temperatures was studied experimentally. Four oxidation stages were identified based on thermogravimetry in the temperature range from 300 to 1500 °C. The analysis of partially oxidized samples recovered from specific intermediate temperatures and a review of the available literature on alumina polymorphs formed at different temperatures were used to suggest the following simplified oxidation sequence. During stage I, from 300 to about 550 °C, the thickness of the natural amorphous alumina layer on the particle surface increases. The rate of this process is controlled by the outward diffusion of Al cations. A transformation of amorphous alumina into γ-Al_2O_3 occurs at about 550 °C, when the oxide layer thickness exceeds the critical thickness of amorphous alumina of ~4 nm. The density of the γ-Al_2O_3 is greater than that of amorphous alumina, and the newly formed γ-Al_2O_3 nanocrystallites produce a monolayer covering the aluminum surface only partially. A bare aluminum surface is produced as a result of the amorphous γ-Al_2O_3 transformation. The oxidation rate increases rapidly during stage II until the γ-Al_2O_3 coverage becomes multilayered and continuous. The growth of a continuous γ-Al_2O_3 layer and its partial transformations into the structurally similar θ-Al_2O_3 polymorph occur during stage III oxidation. The stage ends when the formation of a dense and stable α-Al_2O_3 occurs, resulting in an abrupt decrease in oxidation rate. Finally, oxidation stage IV is characterized by the formation and growth of the α-Al_2O_3 oxide. Qualitative analysis of the rates of oxidation at different stages enables one to understand the wide

range of aluminum ignition temperatures that were observed for particles of different sizes.

Acknowledgments

This work has been supported in part by the Defense Threat Reduction Agency, Award DTRA01-02-C-0064, the U.S. Office of Naval Research, Award N000140010446, and the U.S. Department of the Navy, Crane Division, Award N00164-02-C-4702.

References

[1] K.P. Brooks, M.W. Beckstead, J. Propuls. Power 11 (4) (1995) 769–780.
[2] E.W. Price, Prog. Astronaut. Aeronaut. 90 (1984) 479–513.
[3] E.L. Dreizin, Combust. Flame 105 (1996) 541–556.
[4] S. Yuasa, Y. Zhu, S. Sogo, Combust. Flame 108 (1997) 387–396.
[5] V.I. Rozenband, N.I. Vaganova, Combust. Flame 88 (1) (1992) 113–118.
[6] Y. Zhu, Y. Yuasa, Combust. Flame 115 (3) (1998) 327–334.
[7] I.G. Assovskiy, O.M. Zhigalina, V.I. Kolesnikov-Svinarev, in: Fifth International Microgravity Combustion Workshop, Cleveland, May 18–20, 1999, NASA, 1999.
[8] R. Friedman, A. Macek, Combust. Flame 6 (1962) 9–19.
[9] A.G. Merzhanov, Yu.M. Grigorjev, Yu.A. Galchenko, Combust. Flame 29 (1977) 1–14.
[10] C. Johnson, T. Parr, D. Hanson-Parr, R. Hollins, S. Fallis, K. Higa, in: Proc. 37th JANNAF Combust. Subcomm. Meeting, November 2000, pp. 539–551.
[11] A.G. Alekseev, R.A. Barlas, T.I. Tsidelko, A.F. Shapoval, in: V.V. Nedin (Ed.), Preduprezhdenie Vnezapnykh Vzryvov Gazodispersnykh Sistem, 1971, pp. 66–73 [in Russian].
[12] A.F. Belyaev, Yu.V. Frolov, A.I. Korotkov, Fiz. Goren. Vzryva 4 (3) (1968) 323–329 [in Russian].
[13] C. Brossard, A. Ulas, C.L. Yen, K.K. Kuo, in: 16th International Colloquium on the Dynamic of Explosions and Reactive Systems, Krakow, Poland, August 3–8, 1997.
[14] M.E. Derevyga, L.N. Stesik, E.A. Fedorin, Combust. Explos. Shock Waves 13 (6) (1977) 722–726.
[15] V.A. Ermakov, A.A. Razdobreev, A.I. Skorik, V.V. Pozdeev, S.S. Smolyakov, Fiz. Goren. Vzryva 18 (2) (1982) 141–143 [in Russian].
[16] T.A. Roberts, R.L. Burton, H. Krier, Combust. Flame 92 (1–2) (1993) 125–143.
[17] A.V. Fedorov, Yu.V. Kharlamova, Combust. Explos. Shock Waves 39 (5) (2003) 544–547.
[18] P. George, P.E. DesJardin, in: Proc. ASME Summer Heat Transfer Conference, Las Vegas, 2003, ASME, 2003, pp. 161–168.
[19] V.I. Kiselev, B.M. Leipinskikh, Kinetics of Oxidation of Molten Aluminum, Inst. Metall., Sverdlovsk, Deposited Doc. VINITI 542-74, 1974 [in Russian].
[20] B.S. Mitin, V.V. Samoteikin, Zh. Fiz. Khim. 45 (3) (1971) 730 [in Russian].
[21] E. Bergsmark, C.J. Simensen, P. Kofstad, Mater. Sci. Eng. A 120 (1989) 91–95.
[22] I. Levin, D. Brandon, J. Am. Ceram. Soc. 81 (8) (1998) 1995–2012.
[23] L.P.H. Jeurgens, W.G. Sloof, F.D. Tichelaar, E.J. Mittemeijer, Phys. Rev. B 62 (7) (2000) 4707–4719.
[24] L.P.H. Jeurgens, W.G. Sloof, F.D. Tichelaar, E.J. Mittemeijer, Thin Solid Films 418 (2002) 89–101.
[25] L.P.H. Jeurgens, W.G. Sloof, F.D. Tichelaar, E.J. Mittemeijer, J. Appl. Phys. 92 (3) (2002) 1649–1656.
[26] O.A. Riano, J. Wadsworth, O.D. Sherby, Acta Mater. 51 (2003) 3617–3634.
[27] J.C. Sanchez-Lopez, A.R. Gonzalez-Elipe, A. Fernandez, J. Mater. Res. 13 (3) (1998) 703–710.
[28] P.E. Doherty, R.S. Davis, J. Appl. Phys. 34 (1963) 619–628.
[29] K. Tomas, M.W. Roberts, J. Appl. Phys. 32 (1961) 70–75.
[30] A. Steinheil, Ann. Phys. 19 (5) (1934) 465–483.
[31] J.M. McHale, A. Auroux, A.J. Perrotta, A. Navrotsky, Science 277 (1997) 788–791.
[32] Y.-S. Kwon, A.R. Gromov, A.P. Ilyin, Combust. Flame 131 (3) (2002) 349–352.
[33] A.P. Il'in, A.A. Gromov, G.V. Yablunovskii, Combust. Explos. Shock Waves 37 (4) (2001) 418–422.
[34] A.S. Tompa, R.F. Boswell, P. Skahan, C. Gotzmer, J. Therm. Anal. 49 (3) (1997) 1161–1170.
[35] M.M. Mench, K.K. Kuo, C.L. Yeh, Y.C. Lu, Combust. Sci. Technol. 135 (1988) 269–292.